AD-A082 382 AIR FORCE GEOPHYSICS LAB HANSCOM AFB MA F/G 22/2
CALIBRATION OF THE RAPID SCAN PARTICLE DETECTOR MOUNTED IN THE --ETC(U)
JUL 79 F A HANSER, D A HARDY, B SELLERS
UNCLASSIFIED AFGL-TR-79-0167 NL

END
DATE FILMED
4 80
DTIC

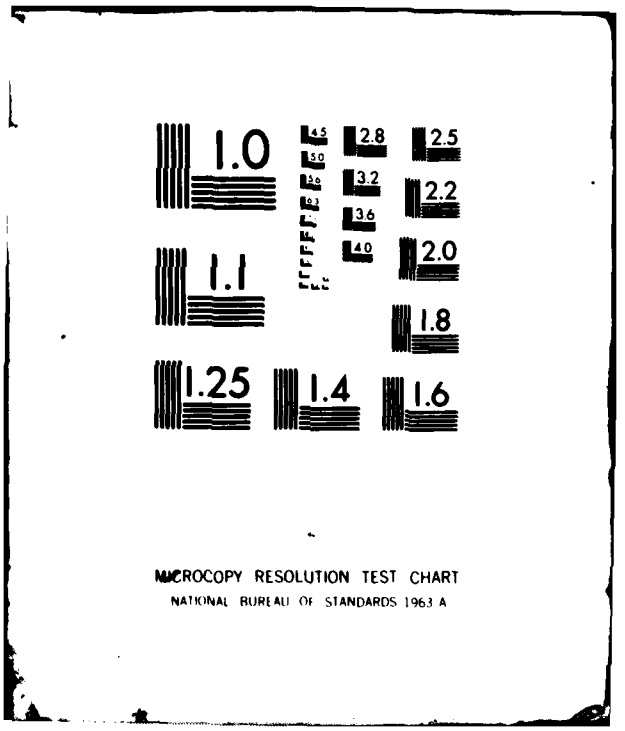
1.0
1.1
1.25
1.4
1.6
1.8
2.0
2.2
2.5
2.8
3.2
3.6
4.0
4.5
5.0
5.6
6.3
MICROCOPY RESOLUTION TEST CHART
NATIONAL BUREAU OF STANDARDS 1963 A

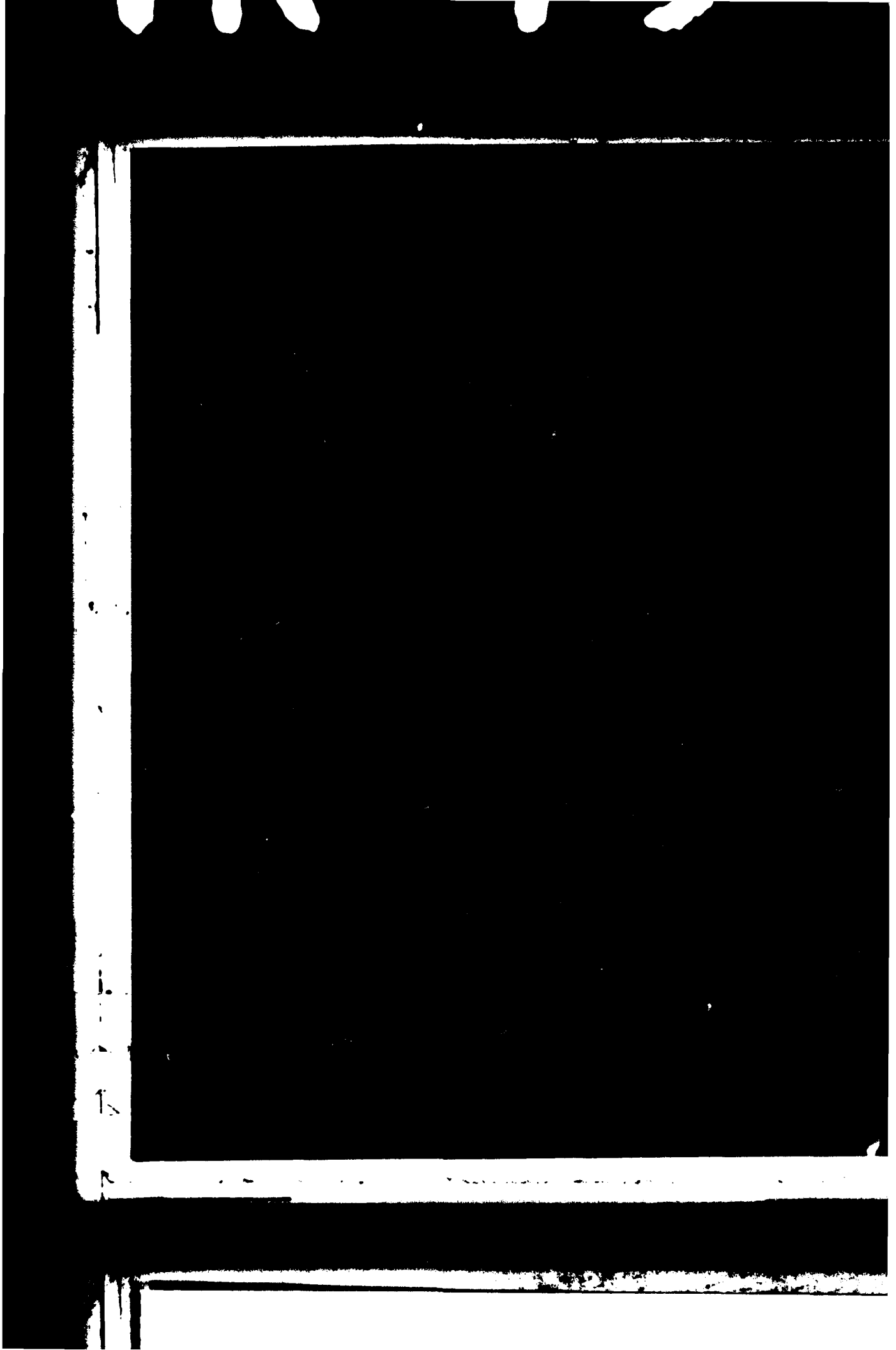

(9) Final rept.,

Unclassified

SECURITY CLASSIFICATION OF THIS PAGE (When Data Entered)

REPORT DOCUMENTATION PAGE	READ INSTRUCTIONS BEFORE COMPLETING FORM
(14) AFGL-TR-79-0167, AFGL-IP-278	3. RECIPIENT'S CATALOG NUMBER
(6) 4. TITLE (and Subtitle) CALIBRATION OF THE RAPID SCAN PARTICLE DETECTOR MOUNTED IN THE SCATHA SATELLITE.	5. TYPE OF REPORT & PERIOD COVERED Scientific. Final
	6. PERFORMING ORG. REPORT NUMBER IP No. 278
(10) 7. AUTHOR(s) Frederick A. Hanser, David A. Hardy, Capt, USAF, Bach Sellers	8. CONTRACT OR GRANT NUMBER(s) (12) 41
9. PERFORMING ORGANIZATION NAME AND ADDRESS Air Force Geophysics Laboratory (PHG) Hanscom AFB Massachusetts 01731	10. PROGRAM ELEMENT, PROJECT, TASK AREA & WORK UNIT NUMBERS (16) 62101F 76610606 (17) 06
11. CONTROLLING OFFICE NAME AND ADDRESS Air Force Geophysics Laboratory (PHG) Hanscom AFB Massachusetts 01731	(11) 18 Jul 1979
	13. NUMBER OF PAGES 41
14. MONITORING AGENCY NAME & ADDRESS(if different from Controlling Office)	15. SECURITY CLASS. (of this report) Unclassified
	15a. DECLASSIFICATION/DOWNGRADING SCHEDULE

16. DISTRIBUTION STATEMENT (of this Report)

Approved for public release; distribution unlimited.

17. DISTRIBUTION STATEMENT (of the abstract entered in Block 20, if different from Report)

18. SUPPLEMENTARY NOTES

*Panametrics, Inc., Waltham, MA
Work was related under Contract F19628-77-C-0137.

19. KEY WORDS (Continue on reverse side if necessary and identify by block number)

Calibration of electron and proton detectors
Electrostatic analyzers and solid state spectrometers
High time resolution spectrum analysis
Electron and proton detectors

20. ABSTRACT (Continue on reverse side if necessary and identify by block number)

A rapid scan particle detector (RSPD) for electrons and protons in the range of 0.05 keV to greater than a few MeV has been designed, constructed, and calibrated. The RSPD uses electrostatic analyzers (ESA's) with Spiraltron electron multipliers (SEM's) for 0.05 to 60 keV particles, and solid-state detector telescopes for the higher energy particles. The ESA's have been extensively calibrated at the Rice University Calibration Facility, using 0.04 to 45 keV electrons and 0.1 to 30 keV ions, and the results

DD FORM 1 JAN 73 1473 EDITION OF 1 NOV 65 IS OBSOLETE

Unclassified

SECURITY CLASSIFICATION OF THIS PAGE (When Data Entered)

4109578

JOB

20. Abstract (Continued)

are given in this report. The calibration procedure for the SSS's is also described, and the results are tabulated.

The RSPD was launched in the SCATHA satellite on 30 January 1979 and is known as the SC5 instrument. Orbit operations have been excellent, with the SSS's operating nearly 100 percent of the time and the ESA's operating about 50 percent of the time. Some SEM degradation has been observed, but 50 percent time operation at a higher bias level is achieving a sufficiently stable operation that should allow reliable data-taking for at least the one-year-design lifetime.

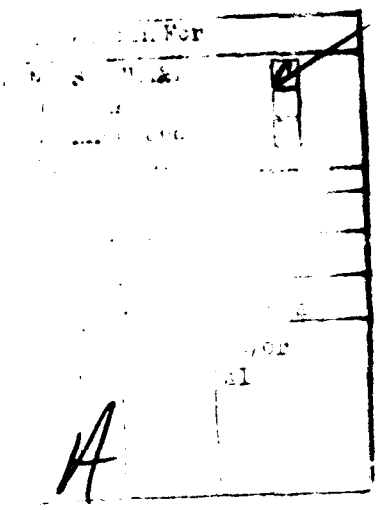

Contents

Illustrations

Tables

Tables

Calibration of the Rapid Scan Particle Detector Mounted in the SCATHA Satellite

1. INTRODUCTION

A rapid scan particle spectrometer (RSPD) for detecting electrons and protons in the range of 0.05 keV to greater than a few MeV has been designed, constructed, and calibrated. The RSPD has been integrated into the Air Force SCATHA (Spacecraft Charging at High Altitudes) satellite to provide high-time-resolution measurements of the electron and proton fluxes as part of a program to study spacecraft charging phenomena. The RSPD is designated as the SC5 instrument on the SCATHA satellite, which was launched successfully on 30 January 1979.

The RSPD uses cylindrical plate electrostatic analyzers (ESA's) with SPIRALTRON electron multipliers (SEM's) for particle detection to cover the 0.05 to 60 keV range, and solid state spectrometers (SSS's) using a solid state detector telescope configuration to cover the 60 keV to few MeV range. Details of the basic design of the RSPD have been given in Refs. 1–3. Also shown in Ref. 3 are the results of detailed scans across the aperture of the Spiraltron multipliers. In order to provide the desired high-time resolution, the energy resolution has been made broad, with the ESA energy channels having about 50 percent width.

(Received for publication 17 July 1979)

Due to the limited space available, references 1 to 3 will not be listed here. See References, page 31.

The geometric factors of the ESA's depend on the transmission factors of the analyzer plates and on the detection efficiency of the SEM's. Electron multiplier efficiencies have been measured for electrons (Refs. 4–6) and protons (Refs. 7, 8) but show significant variations when measured by different groups, and even from one unit to another. There is thus a significant variability (at least ±50 percent) in the SEM detection efficiency, and this, coupled to the uncertainty in calculating the transmission factors for the broad-resolution ESA plate geometry, makes it necessary to calibrate the ESA's if better than 50 percent accuracy is desired.

The RSPD was taken to the electron-proton calibration facility at Rice University and calibrated in electron beams of 0.04 to 45 keV, and proton beams of 0.1 to 30 keV. This gave a reasonably precise measurement of the G(E) curves for most of the ESA channels, and sufficient data to allow extrapolation to higher and lower energies. The lowest energy electron SSS channels, where the efficiency is affected by backscattering from the aluminum light and proton shield, also had correction factors measured to allow calculation of the correct G(E) factors.

In the following sections, the RSPD is described in greater detail, the particle calibration procedures are presented, and the ESA calibration results are shown in both graphical and tabular form. Some results on UV sensitivity of the ESA's are presented, and the SSS calculated G(E) factors are given, corrected by the calibration data for the lowest energy electron channels.

2. THE RAPID SCAN PARTICLE SPECTROMETER – SUMMARY DESCRIPTION

The RSPD outline is shown in Figure 1. Two complete sets of spectrometers are included, one set oriented parallel (∥) to the spacecraft spin axis, and one set perpendicular (⊥) to the spin axis. The ⊥ set includes a photodiode to allow the SEM high voltages to be turned off when the ⊥ ESA's are viewing the sun and responding to scattered solar UV.

---

4. Archuleta, R.J., and DeForest, S.E. (1971) Efficiency of channel electron multipliers for electrons of 1-50 keV, Rev. Sci. Inst. 42:89.

5. Bordoni, F. (1971) Channel electron multiplier efficiency for 10-1000 eV electrons, Nucl. Inst. Meth. 97:405.

6. Arnoldy, R.L., Isaacson, P.O., Gats, D.F., and Choy, L.W. (1973) The calibration of electrostatic analyzers and channel electron multipliers using laboratory simulated omnidirectional electron beams, Rev. Sci. Inst. 44:172.

7. Iglesias, G.E., and McGarity, J.O. (1971) Channel electron multiplier efficiency for protons of 0.2-10 keV, Rev. Sci. Inst. 42:1728.

8. Egidi, A., Marconero, R., Pizzella, G., and Sperli, F. (1969) Channeltron fatigue and efficiency for protons and electrons, Rev. Sci. Inst. 40:88.

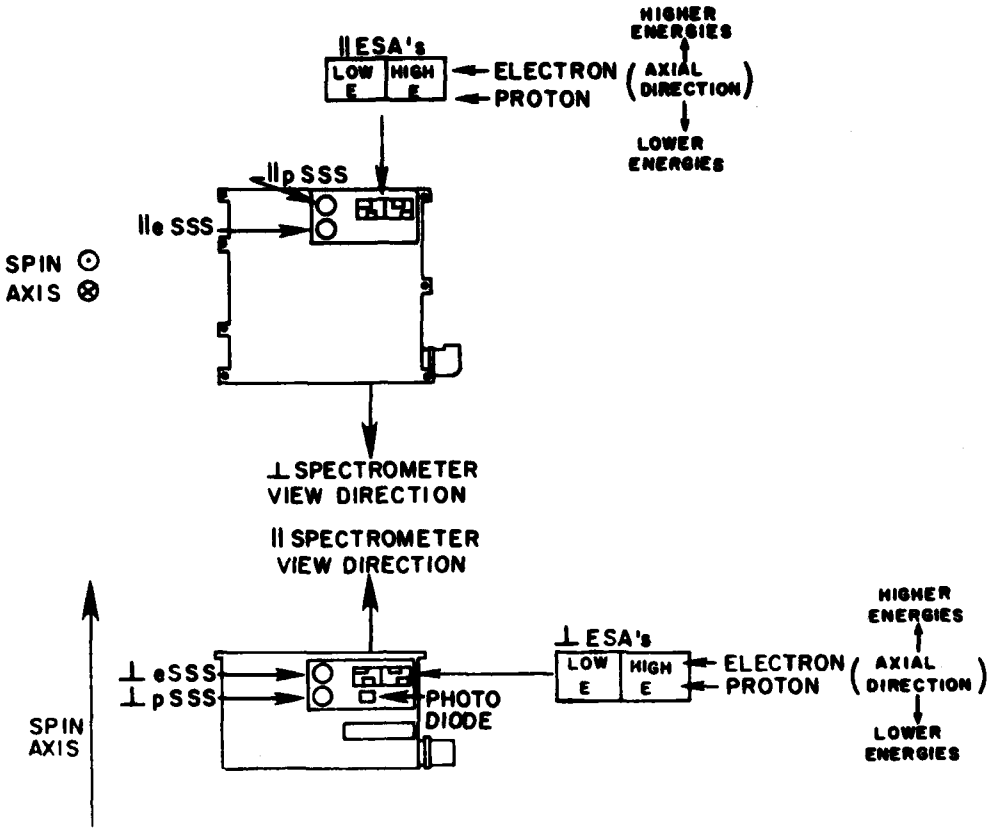

Figure 1. Outline of the RSPD Showing the Spectrometer Apertures

The low energy electrons and protons (0.05 to 60 keV) are detected by cylindrical plate ESA's with SEM's. The basic design of a dual (electron and proton) ESA unit is shown in Figure 2. Each spectrometer set (∥ and ⊥) includes two ESA units, one for low energy (LE) (0.05-1.7 keV) and one for higher energy (HE) (1.7–60 keV) particles. Each ESA measures particles in four energy channels of about 50 percent energy resolution, and in one background channel with 0 volts on the deflection plate. Since each measurement takes 0.2 sec, a complete ESA spectrum is measured in 1 sec.

The high energy electrons and protons (60 keV to a few MeV) are measured by solid state detector telescopes. The basic design of the solid state spectrometers is shown in Figure 3. The electron SSS's use a 0.1 mil Al foil to absorb light and protons below about 250 keV, and have a 300-μ thick front detector. The proton SSS's use a sweeping magnet to eliminate electrons below a couple hundred keV and an approximately 6-μ thick front detector with 120 $\mu g/cm^2$ of Al for a

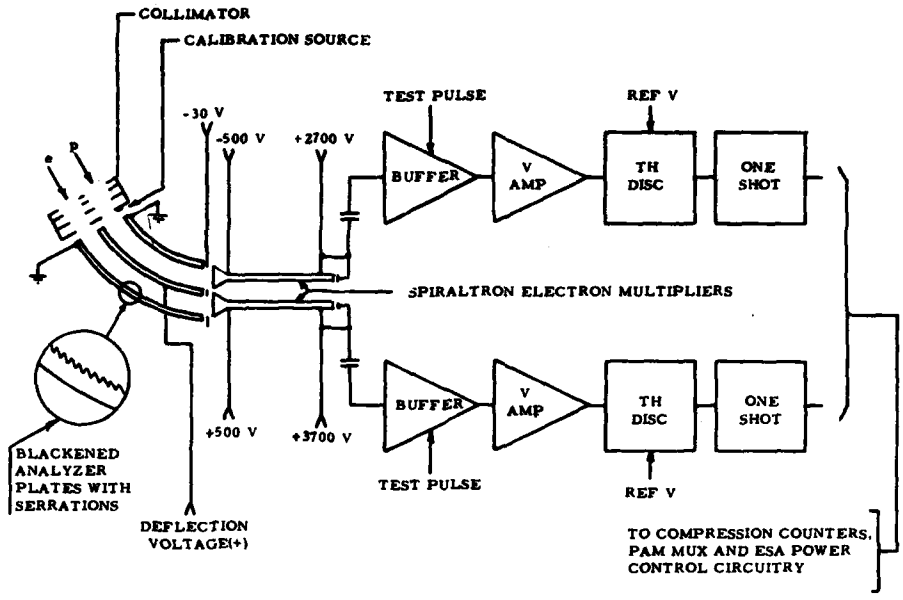

Figure 2. Basic Design of the Dual Electrostatic Analyzer Unit

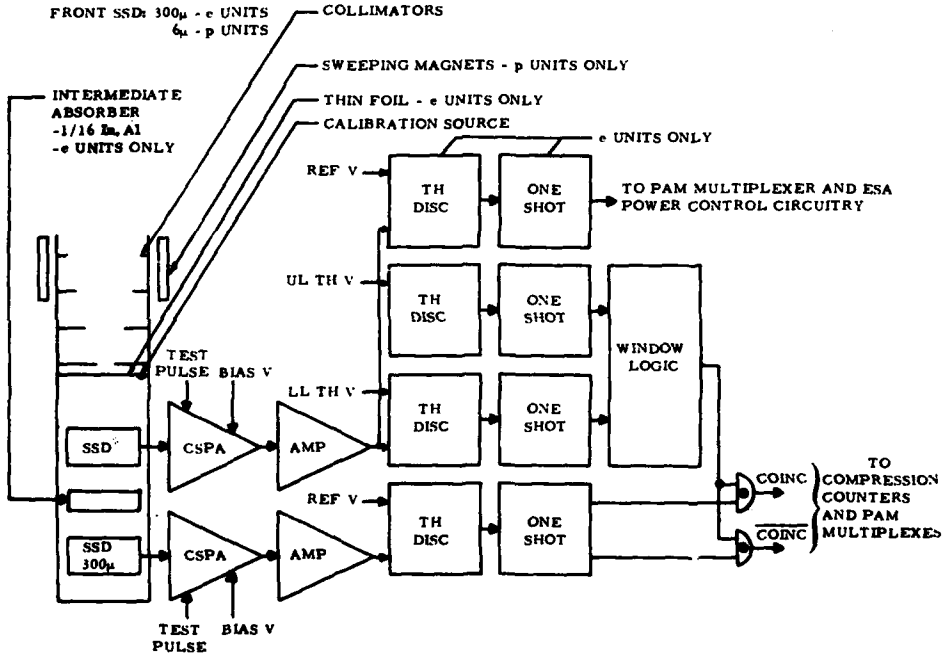

Figure 3. Basic Design of the Solid State Spectrometers

light shield. The front detector in anticoincidence with the rear detector measures lower energy particles (30 to 550 keV for electrons, 100 to about 500 keV for protons), while the two detectors in coincidence cover the higher energy range particles (550 to >1000 keV for electrons, about 500 to 8000 keV for protons). The SSS's make a complete 10-point spectral measurement once every second.

The RSPD has many operating modes in addition to the 1-sec spectral scan, and these are detailed in Refs. 1 and 2. The remainder of this report describes the detailed calculation and calibration of the response of the RSPD to electrons and protons.

3. CALIBRATION PROCEDURE

The Rice University electron/proton calibration facility uses a 3-ft-diam by 6-ft-long cylindrical vacuum chamber pumped by a liquid-nitrogen-trapped, diffusion pump. The unit being calibrated is mounted on a double axis rotatable fixture that is computer-controlled to map out the acceptance cone.

An electron beam was generated from a polished Al plate illuminated by Hg lamps, with the desired negative voltage applied to the Al plate. Helmholz coils were used to reduce the effects of the earth and stray magnetic fields. A baffle was used over the ground exit plane to eliminate lower energy electrons at large angles, which come from some of the intermediate drift tube rings.

A proton beam came from a heated filament followed by a magnetic mass analyzer. A positive voltage applied to the filament circuit provided the required proton energy. Since the proton beam was only about 1 in. in diameter, the proton ESA aperture had to be centered in the beam.

A calibration run for a particular ESA set to a fixed energy channel was started with a Faraday cap in the beam to provide the absolute flux measurement, after which the RSPD was swung into position for the computer-controlled scan. Typically, a scan covered a $\pm 20^{\circ}\theta$, $\pm 20^{\circ}\phi$ range, in 2° steps, and required about 7 min.

The electron beam was usable down to about 40 eV, although this required careful adjustment of the Helmholtz coils. The maximum electron energy was 45 keV, limited by corona arcing inside the vacuum chamber. For protons it was possible to obtain a usable 100 eV beam, with the maximum being 30 keV, limited by arcing.

The computer output for each run was a listing of the detailed response vs the (θ, ϕ) angles, and a summary giving the geometric factor. The four ESA's and two SSS's (anticoincidence channels) in a given direction ($\parallel$ or $\perp$) were all done simultaneously in the electron beam. Only one proton ESA could be done at any time in

the proton beam. Typical count times for each angle position were 0.1 sec, accumulating about 1000 counts in the peak.

All of the ESA's were calibrated for a wide range in electron energies, and the proton ESA's were calibrated with protons. Some Electron SSS data were obtained in the two lowest energy channels. Results are described in more detail in the following sections.

4. ESA CALIBRATION RESULTS

4.1 Electron ESA's

The calibration data for the ∥ electron ESA's are given in Figure 4, and the data for the ⊥ electron ESA's in Figure 5. During the final calibration of the flight unit, some difficulty was encountered with the ⊥ low energy (LE) electron ESA, so the ⊥ LE ESA unit was replaced with the backup ∥ LE ESA unit, and this is reflected in the data.

The shape of the ESA responses in the different energy channels is determined primarily by the ESA geometry and the deflection plate voltage. By normalizing the electron energy to the plate voltage and the peak geometric factor to some standard, the normalized geometric factors for the ∥ (LE and HE) and ⊥ (LE and HE) electron ESA's were obtained and are plotted in Figures 6 and 7. The normalizing factors used are given in Table 1.

The results in Figures 6 and 7 show that the LE electron ESA's have a peak shape nearly independent of the central peak energy, while the HE electron ESA's have a spreading of the width of the peak as the energy increases. This is most likely caused by the greater ability of a high energy electron to scatter once or more and still have enough energy to reach the SEM. This behavior is expected, and shows the importance of calibration for the higher energy channels. The smoothed response curves in Figures 6 and 7 were used to extrapolate the measured responses in Figures 4 and 6 as well as to provide the smoothed response curves shown in the region where data are available.

Tables A1 to A8 list numerical values of G(E) for the electron (and proton) ESA's. The listed values are a combination of the measured values and the smoothed curves in Figures 4 and 5. The geometric factors for the background channel (no. 0) are given in Table 2. The electron ESA's are also sensitive to protons above about 1 keV, with G(E) of a few x 10^{-7} cm^2-sr. The precise value and shape of this proton sensitivity was not measured, but is is significantly lower than the electron sensitivity of channel 0.

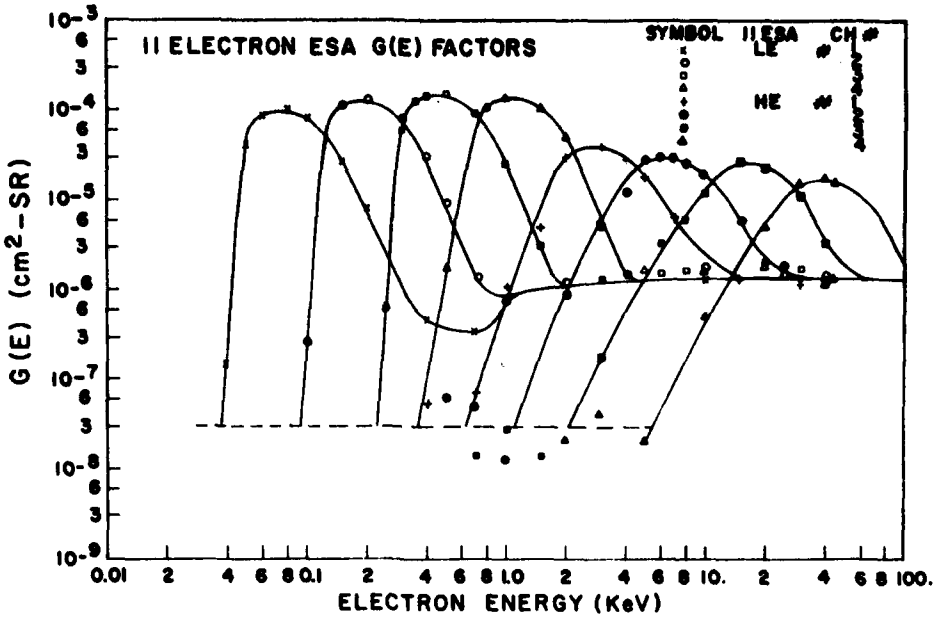

Figure 4. Calibration Data and Smoothed Response Curves for the Parallel Electron ESA's

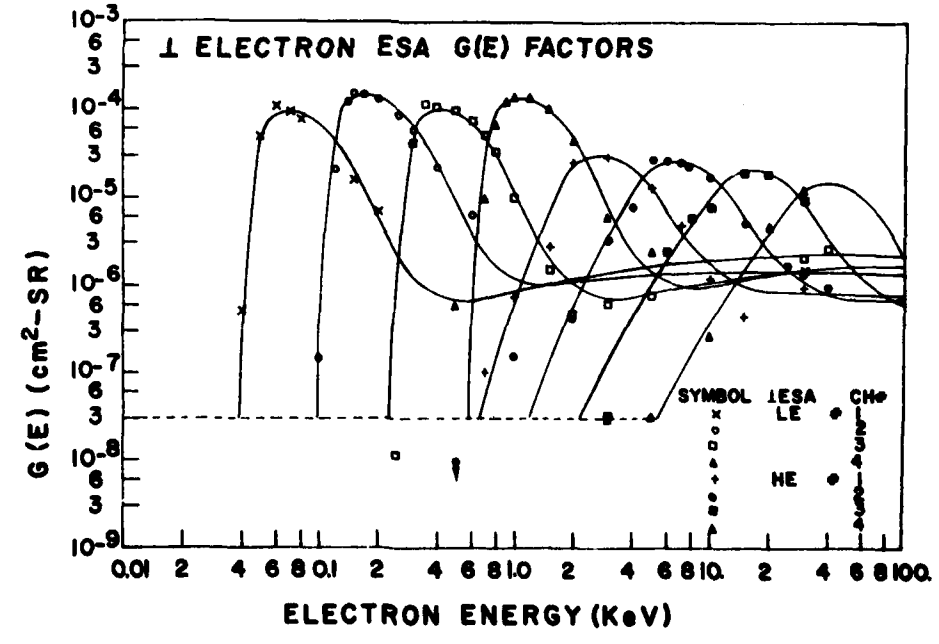

Figure 5. Calibration Data and Smoothed Response Curves for the Perpendicular Electron ESA's

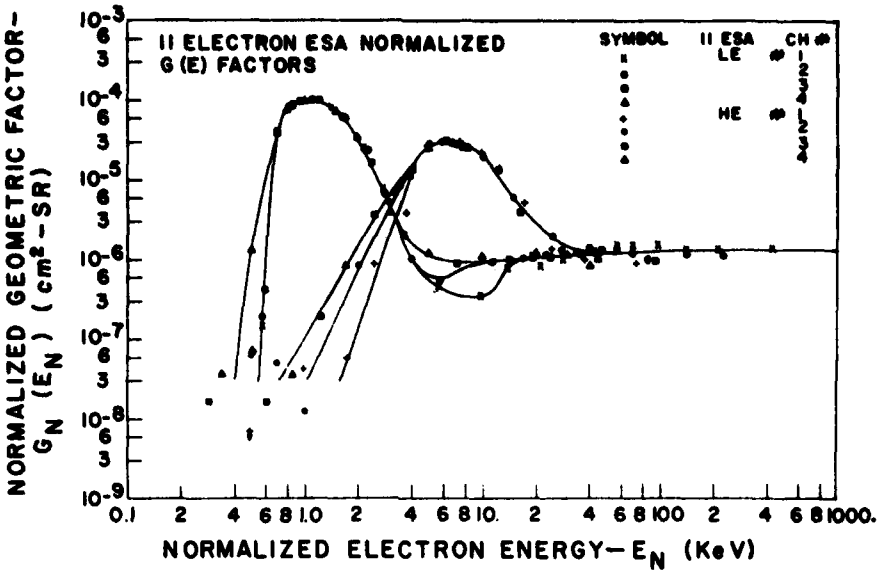

Figure 6. Normalized Geometric Factors for the Parallel LE and HE Electron ESA's

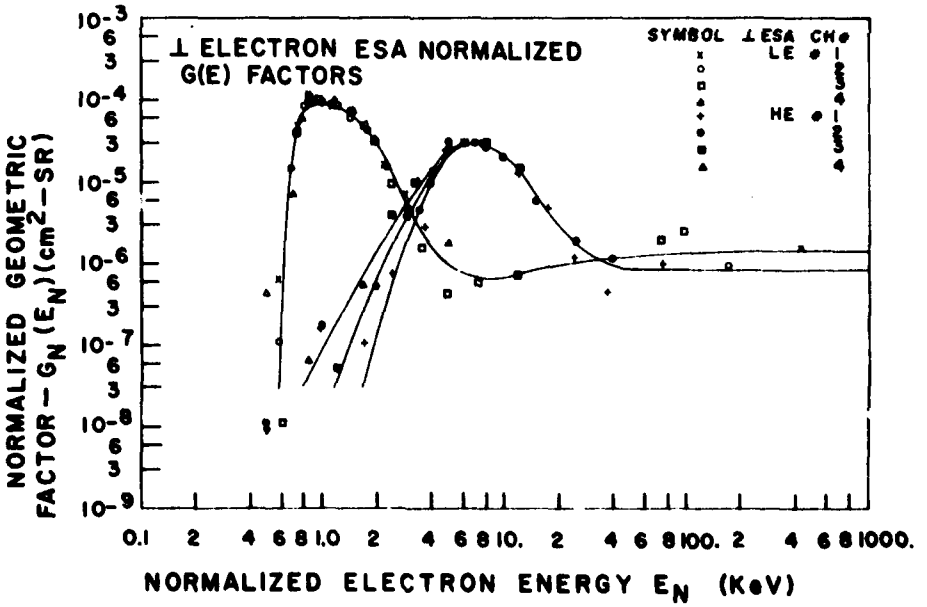

Figure 7. Normalized Geometric Factors for the Perpendicular LE and HE Electron ESA's

Table 1. Conversion Factors for Normalized Geometric Factors for Electron ESA's

ESA Type/Energy Channel	Energy Normalization Factor	Geometric Factor Normalization for: ∥ Electron ESA's	Geometric Factor Normalization for: ⊥ Electron ESA's
LE		(to 1.00×10^{-4} cm^2-sr)	
1	14.1	1.00	1.00
2	5.67	0.77	0.67
3	2.37	0.68	0.91
4	1.00	0.71	0.71
HE		(to 3.00×10^{-4} cm^2-sr)	
1	2.46	0.79	1.00
2	1.00	1.00	1.15
3	0.406	1.15	1.58
4	0.170	1.71	2.00

Table 2. ESA Geometric Factors -- Energy Channel No. 0

Particle Energy (keV)	LE ESA G(E)*		LE ESA G(E)*	
	Electron	Proton	Electron	Proton
0.1	1.-8	1.-8	1.-8	1.-8
0.3	8.-8	3.-8	2.-8	3.-8
1.0	8.-7	6.-7	2.-7	3.-7
3.	1.7-6	1.2-6	6.-7	1.-6
10.	1.4-6	1.7-6	1.-6	1.2-6
30.	1.6-6	1.5-6	1.-6	1.0-6

*G(E) in cm^2-sr; 1.-8 ≡ $1. \times 10^{-8}$, etc.

The high energy tails shown for all the electron ESA channels may possibly be only upper limits. For these tails to be accurate, the electron beam must be monoenergetic to much less than 1 percent contamination. This was not directly measured, and measurements without the ground-plane baffle showed significant contamination at low energy and large angles.

The accuracy of the peaks in the G(E) curves is estimated to be about 25 percent. This is based on the observed variations in electron flux measured by the electrometer before and after each run, on the electrometer absolute accuracy, and primarily on the subtraction of background from the electrometer current reading.

A summary of the electron ESA characteristics is given in Table 3. The values for $\bar{G}\Delta E$ were calculated for a flat electron spectrum, but only over the peak in the G(E) curve. The $\bar{G}\Delta E$ values are useful for first-order estimates of the electron spectrum. A precise estimate of the electron spectrum requires more extensive fitting, using the detailed shape of the G(E) curves.

Table 3. Summary of Electron ESA Detection Characteristics

ESA /Ch No.	Flat spectrum calculation			From response curves		
	$\bar{E}$ (keV)	ΔE(FWHM) (keV)	$\bar{G}\Delta E$ (cm^2-sr-keV)	E_{peak} (keV)	$\bar{E}$(1/2 ht) (keV)	ΔE(1/2 ht) (keV)
∥ESA's						
LE/#1	0.112	0.138	8.5×10^{-6}	0.073	0.089	0.077
" /#2	0.27	0.30	2.8×10^{-5}	0.18	0.22	0.19
" /#3	0.68	0.87	7.7×10^{-5}	0.44	0.53	0.44
" /#4	1.50	1.55	1.65×10^{-4}	1.05	1.26	1.08
HE/#1	4.6	6.2	1.46×10^{-4}	2.7	3.2	2.7
" /#2	9.0	8.9	2.4×10^{-4}	6.3	7.6	7.2
" /#3	23.	25.	5.4×10^{-4}	16.	20.	19.
" /#4	53.	53.	8.3×10^{-4}	40.	47.	47.
⊥ESA's						
LE/#1	0.110	0.160	7.0×10^{-6}	0.070	0.084	0.067
" /#2	0.26	0.33	2.7×10^{-5}	0.18	0.21	0.17
" /#3	0.62	0.78	4.7×10^{-5}	0.42	0.49	0.38
" /#4	1.57	1.64	1.52×10^{-4}	1.10	1.22	1.12
HE/#1	4.4	5.7	1.06×10^{-4}	2.7	3.3	3.0
" /#2	9.2	9.1	2.1×10^{-4}	6.7	8.0	7.6
" /#3	24.	26.	4.3×10^{-4}	17.	20.	19.
" /#4	54.	55.	7.1×10^{-4}	49.	47.	46.

4.2 Proton ESA's

The calibration data for the ∥ and ⊥ proton ESA's are given in Figures 8 and 9. The lowest energy usable proton beam was 0.1 keV and the highest was 30 keV, so the proton ESA calibrations require more use of the smoothed response curves for the highest and lowest energy channels. The ⊥ LE proton ESA is the replacement unit, which was not as extensively calibrated, as shown by the data points in Figure 9.

The normalized geometric factors for the ∥ and ⊥ proton ESA's are given in Figures 10 and 11, and the normalizing factors are listed in Table 4. The proton HE ESA's do not show the spreading that the electron ESA's display because

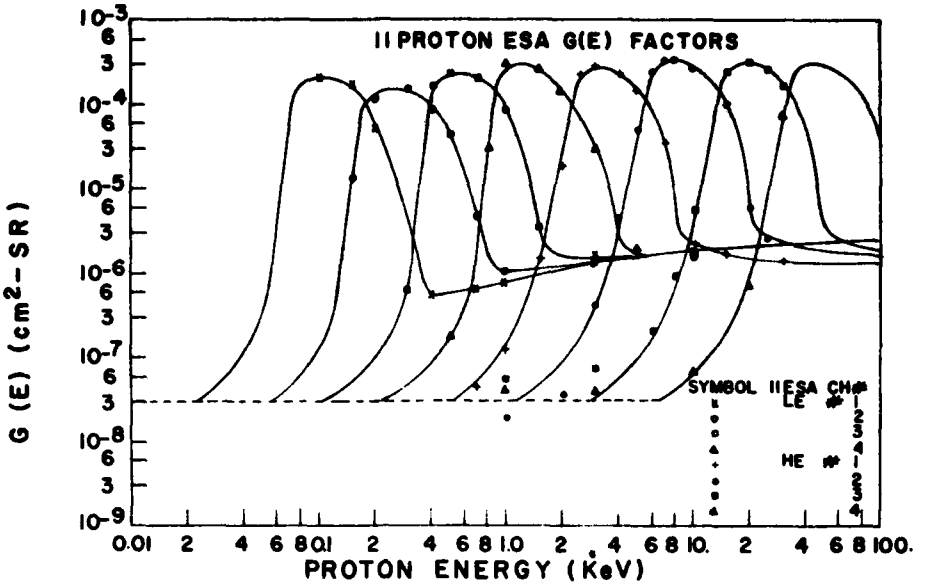

Figure 8. Calibration Data and Smoothed Response Curves for the Parallel Proton ESA's

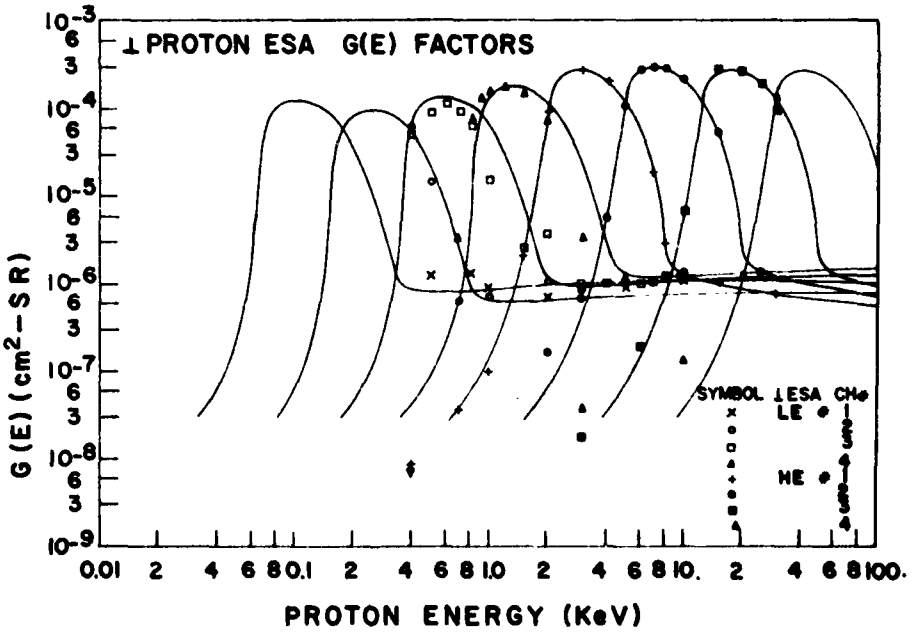

Figure 9. Calibration Data and Smoothed Response Curves for the Perpendicular Proton ESA's

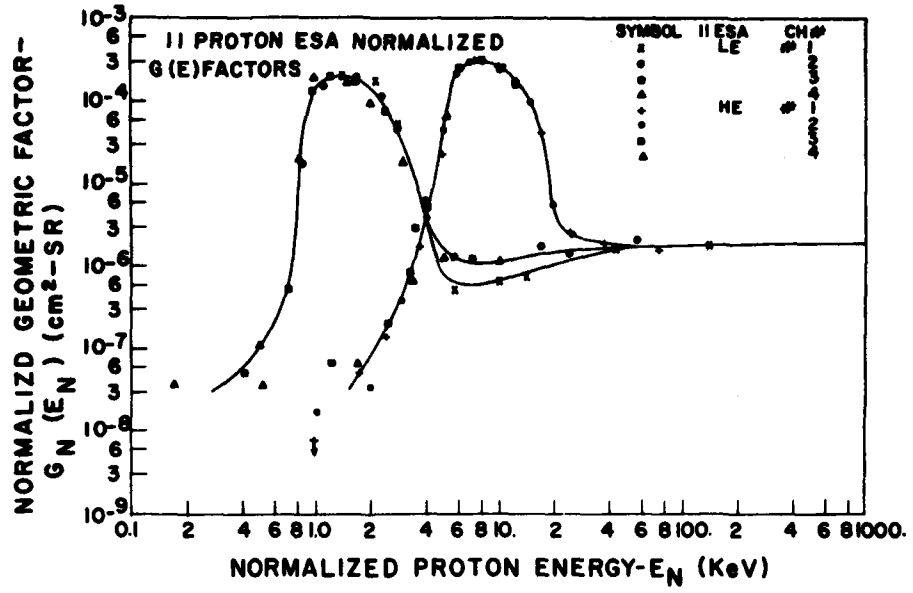

Figure 10. Normalized Geometric Factors for the Parallel LE and HE Proton ESA's

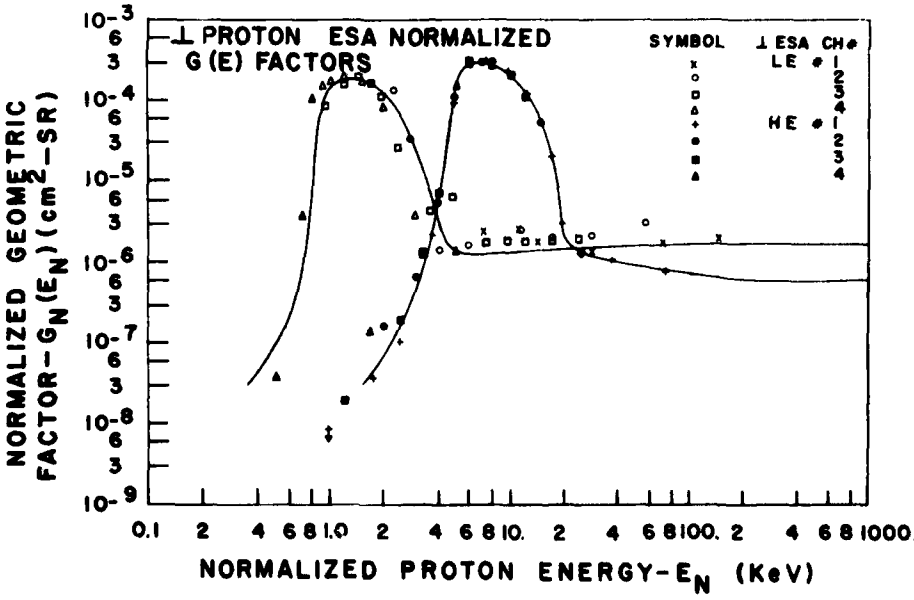

Figure 11. Normalized Geometric Factors for the Perpendicular LE and HE Proton ESA's

Table 4. Conversion Factors for Normalized Geometric Factors for Proton ESA's

ESA Type/Energy Channel	Energy Normalization Factor	Geometric Factor Normalization for: ∥ Proton ESA's	⊥ Proton ESA's
LE		(to 2.00×10^{-4} cm^2-sr)	
1	14.1	1.00	1.82
2	5.67	1.29	2.17
3	2.37	0.83	1.67
4	1.00	0.65	1.11
HE		(to 3.00×10^{-4} cm^2-sr)	
1	2.46	1.11	1.00
2	1.00	0.94	0.94
3	0.406	0.94	1.00
4	0.170	0.94	1.00

protons scatter much less than electrons. The HE proton channels show only small changes in peak efficiency, and so can be readily calibrated in all channels if only one channel is directly calibrated. This comes about because of the constant SEM efficiency vs proton energy at high energy (>1 keV) (Refs. 6, 7).

The sensitivities of the proton ESA's to electrons are shown in Figures 12 and 13. These are greater than the proton sensitivities of the electron ESA's because of the greater scattering of electrons.

The numerical values of G(E) for the proton ESA's are given in Tables A1 to A8. The listed values are a combination of the measured values and the smoothed curves in Figures 8 and 9. The G(E) factors for energy channel 0 (background) are listed in Table 2.

The measured G(E) values are accurate to about ±25 percent. This is due primarily to variations in the proton beam during a calibration run as measured by the electrometer current before and after each run. Because the proton beam was run at higher current levels, background subtraction was not as critical as with the electron beam.

A summary of the proton ESA characteristics is given in Table 5. The values for $\bar{G}\Delta E$ were calculated for a flat proton spectrum over the peak in G(E), ignoring the high energy tail. The $\bar{G}\Delta E$ is only for a first order estimate of the spectrum, with a precise estimate requiring fitting using the detailed shape of G(E).

A detailed tabular listing of the ESA geometric factors, taken partly from the directly measured values and partly from the smoothed curves, is given in

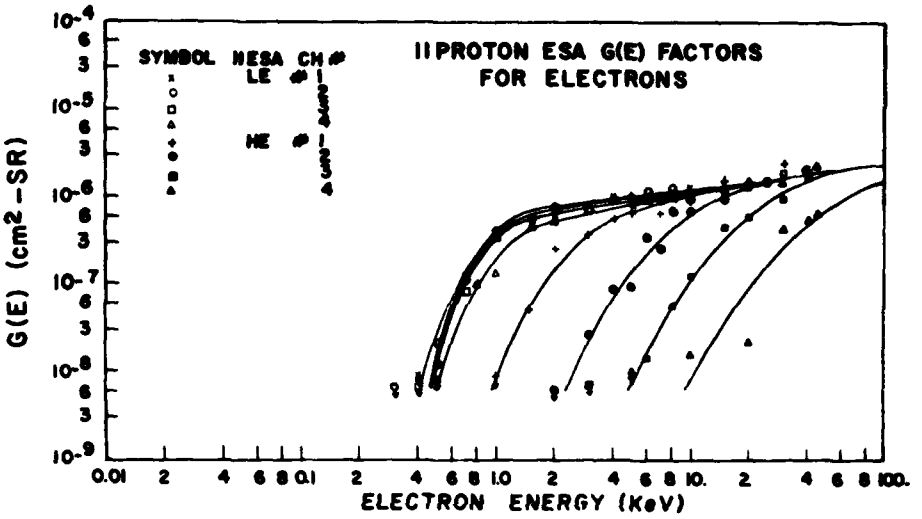

Figure 12. Electron Sensitivities of the Parallel Proton ESA's

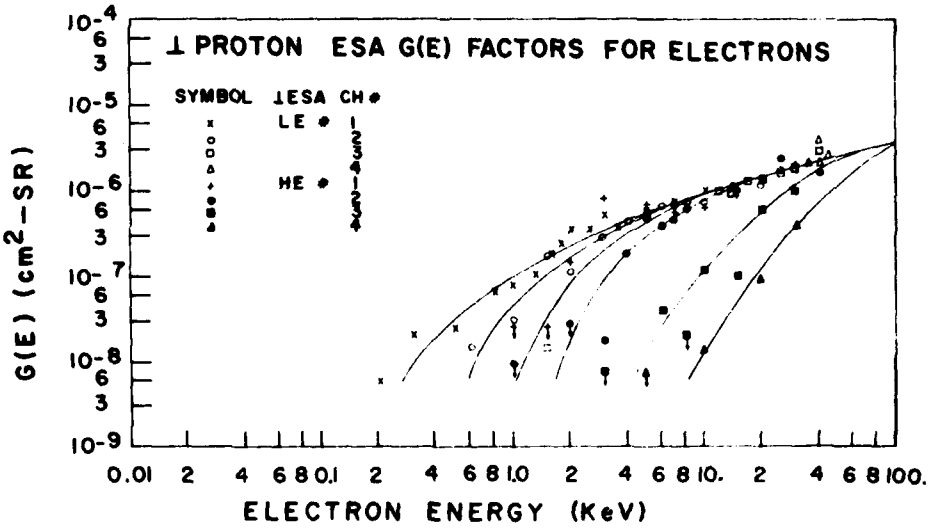

Figure 13. Electron Sensitivities of the Perpendicular Proton ESA's

Table 5. Summary of Proton ESA Detection Characteristics

ESA /Ch No.	Flat spectrum calculation			From response curves		
	$\bar{E}$ (keV)	ΔE(FWHM) (keV)	$\bar{G}\Delta E$ (cm^2-sr-keV)	E_{peak} (keV)	$\bar{E}$(1/2 ht) (keV)	ΔE(1/2 ht) (keV)
∥ESA's						
LE/#1	0.145	0.134	2.4×10^{-5}	0.10	0.125	0.105
" /#2	0.35	0.34	4.3×10^{-5}	0.25	0.30	0.27
" /#3	0.78	0.79	1.38×10^{-4}	0.55	0.67	0.56
" /#4	1.70	1.57	3.7×10^{-4}	1.20	1.44	1.12
HE/#1	4.5	4.3	8.9×10^{-3}	3.1	3.8	2.9
" /#2	10.4	8.1	2.5×10^{-3}	7.8	9.5	7.3
" /#3	25.	20.	5.8×10^{-2}	19.	23.	18.
" /#4	60.	47.	1.37×10^{-2}	44.	55.	43.
⊥ESA's						
LE/#1	0.148	0.148	1.39×10^{-5}	0.10	0.122	0.101
" /#2	0.34	0.33	2.6×10^{-5}	0.24	0.30	0.25
" /#3	0.84	0.86	8.9×10^{-4}	0.56	0.68	0.56
" /#4	1.80	1.62	2.6×10^{-4}	1.3	1.57	1.31
HE/#1	4.0	3.9	8.5×10^{-3}	2.9	3.4	2.6
" /#2	9.7	7.8	2.3×10^{-3}	7.3	8.3	6.6
" /#3	23.	19.	5.0×10^{-2}	18.	21.	16.
" /#4	55.	45.	1.16×10^{-2}	43.	49.	39.

Tables A1 to A8 and in Table 2. The LE ESA G(E) factors for energy channels 1 to 4 are given in Tables A1 to A4, and for the HE ESA's in Tables A5 to A8. The background channel (no. 0) G(E) factors are given in Table 2. In all these tables the G(E) factors are: electron ESA for electrons, proton ESA for protons. The cross-particle G(E) factors are given in Figures 12 and 13 for the proton ESA G(E)'s for electrons, while the electron ESA's have G(E)'s for protons on the order of $10^{-7}cm^2$-sr.

One additional characteristic of the ESA's is given in Figure 14, which shows the variation of arrival direction with energy relative to the central energy of the channel. This curve is an average of several data sets, with different ESA's and energy channels not deviating much from the average. The arrival angles change in the directions shown in Figure 1, with the ⊥ ESA's having angular changes with respect to the spin axis. Because the G(E) factor peaks at the central energy, the effect will only be important for very sharp angular/energy distributions of particles.

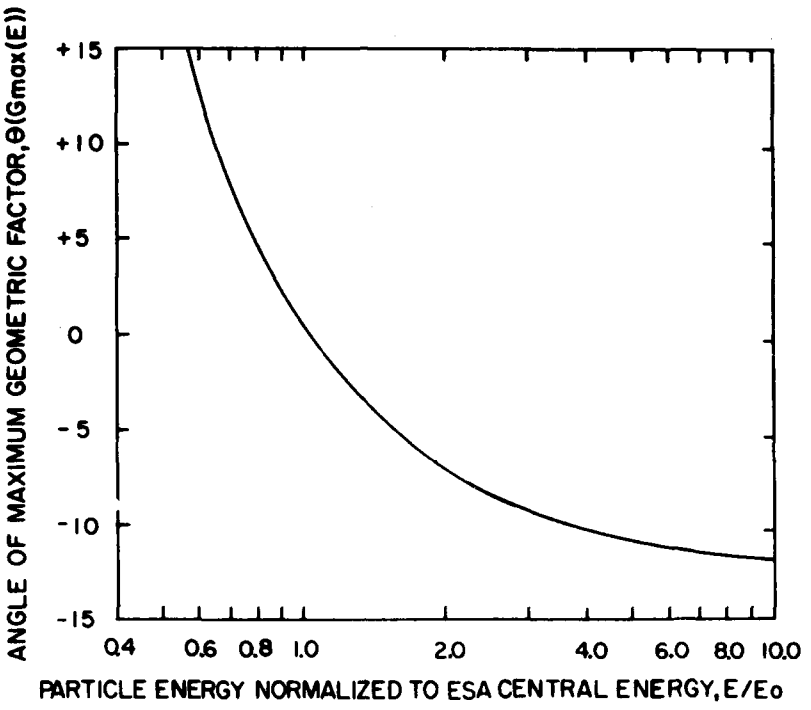

Figure 14. Variation of Particle Arrival Directions With Energy Relative to the ESA Central Energy

4.3 UV Sensitivity Measurements

The UV sensitivity of an engineering model ESA was measured during the design phase of the RSPD and indicated that solar UV (mainly hydrogen Lyman alpha) would produce about a 10 kHz count rate while the ESA was directed at the sun (Refs. 1, 2). The measured response width was about 20°, so the flight unit was designed with a photodiode to permit turning the SEM high voltages off for about 30° of rotation when the $\perp$ ESA's were viewing the sun.

The UV response of the $\perp$ ESA's in the flight RSPD was measured in the Rice University calibration chamber, using a Kr Lamp. The Kr lamp emits primarily at 1236Å ($\simeq$ 85 percent) and at 1165Å ($\simeq$ 15 percent), while solar Lyman alpha is at 1216Å. The Kr lamp output was calibrated by measuring the photoelectron current from a polished Al surface in a Faraday cup arrangement. Using nominal values for the Al photoelectron efficiency, this should given the lamp output to ±50 percent. The $\perp$ HE ESA's were located in the direct beam, while the $\perp$ LE ESA's were about 10° off the beam axis. The ESA's were scanned $\pm 20^{\circ}$ in one direction and $\pm 14^{\circ}$ in the other.

The measured UV responses were about 20° wide for full-width-half-maximum, so the 30° photodiode covers the entire main central response. The peak count rates were about 6 to 9 kHz for the proton ESA's, and 1.5 to 4 kHz for the electron ESA's, with all count rates normalized to an equivalent solar Lyman alpha intensity of 3.1×10^{11} photons/(cm^2-sec). These count rates are in reasonable agreement with the earlier estimates (Refs. 1, 2) for the proton ESA's, and also for the electron ESA's when the reduced collimator area over the SEM's is taken into account. The measured UV count rates are thus about as expected from early design tests, and the photodiode should be able to eliminate most of the solar UV counts when enabled in the automatic shutoff mode.

5. SSS CALIBRATION RESULTS

5.1 Electron SSS G Factors

The electron SSS (solid state spectrometer) illustrated in Figure 3 is a solid state detector telescope with the G factor determined by an inner collimator of 0.201-cm diam and an outer collimator of 1.00-cm diam, separated by 2.65 cm. Using the product of the areas divided by the square of the separation, this gives $G = 3.55 \times 10^{-3} cm^2$-sr for electrons detected with unit efficiency.

The logic configurations for the 10 electron SSS channels are given in Table 6, along with the calculated electron energy ranges based on straight energy losses calculated from the silicon and aluminum stopping powers in Refs. 9 and 10. The five "coincidence" channels (C0 to C4) are not all true coincidence channels, as shown by the logic configurations, but are all labeled as "C" channels for convenience. The coincidence channels have been designed to provide a differential and integral flux measurement at about 1 MeV, and this is the reason for the 1/16 in. Al absorber in Figure 3.

The electron channels in Table 6 do not all have unit detection efficiency because of multiple and back scattering of electrons by the 0.1 mil Al foil. The basic properties of electron transmission by foils and the response of Si detectors to electrons are described in Refs. 11, 12, and 13. The application of the calculations to the present electron SSS is, however, extremely difficult, requiring detailed Monte Carlo calculations for the actual SSS geometry. A much simpler procedure is direct calibration. This has been done with electrons up to 45 keV at the Rice University Calibration Facility. The results are plotted in Figure 15, where a semi-log scale has been used to allow extrapolation to higher energies. The resulting correction factors and $G_{eff}(E)$ are listed in Table 7.

Because of the large number of references cited above, they will not be listed here. See References, page 31.

Table 6. Detection Energy Ranges for Electron SSS

Channel No.	Logic Configuration*	Nominal Electron Energy Range (keV)
Anticoincidence		
A0	$F_1 \cdot \bar{F}_2 \cdot \bar{R}_1$	30-45
A1	$F_2 \cdot \bar{F}_3 \cdot \bar{R}_2$	45-70
A2	$F_3 \cdot \bar{F}_4 \cdot \bar{R}_1$	70-120
A3	$F_4 \cdot \bar{F}_6 \cdot \bar{R}_1$	120-550
A4	$F_5 \cdot \bar{F}_6 \cdot \bar{R}_2$	170-265
Coincidence		
C0	$F_1 \cdot R_1$	>950
C1	$F_2 \cdot R_2$	980-1100
C2	$F_3 \cdot \bar{R}_1$	70-950
C3	R_1	>950
C4	R_2	980-1100

*The front (F) and rear (R) detector thresholds are, in keV: F_1=25, F_2=41, F_3=67, F_4=118, F_5=168, F_6=300, R_1=50, R_2=150.

Table 7. Effective Electron G Factors for SSS

Incident Electron Energy (keV)	Correction Factor	$G_{eff}(E)$ (cm^2-sr)
30	0.05	1.78×10^{-4}
35	0.20	7.1×10^{-4}
40	0.28	9.9×10^{-4}
45	0.35	1.24×10^{-3}
50	0.45	1.60×10^{-3}
60	0.57	2.02×10^{-3}
70	0.67	2.38×10^{-3}
80	0.74	2.63×10^{-3}
90	0.80	2.84×10^{-3}
100	0.85	3.02×10^{-3}
110	0.88	3.12×10^{-3}
120	0.91	3.23×10^{-3}
>120	1.00	3.55×10^{-3}

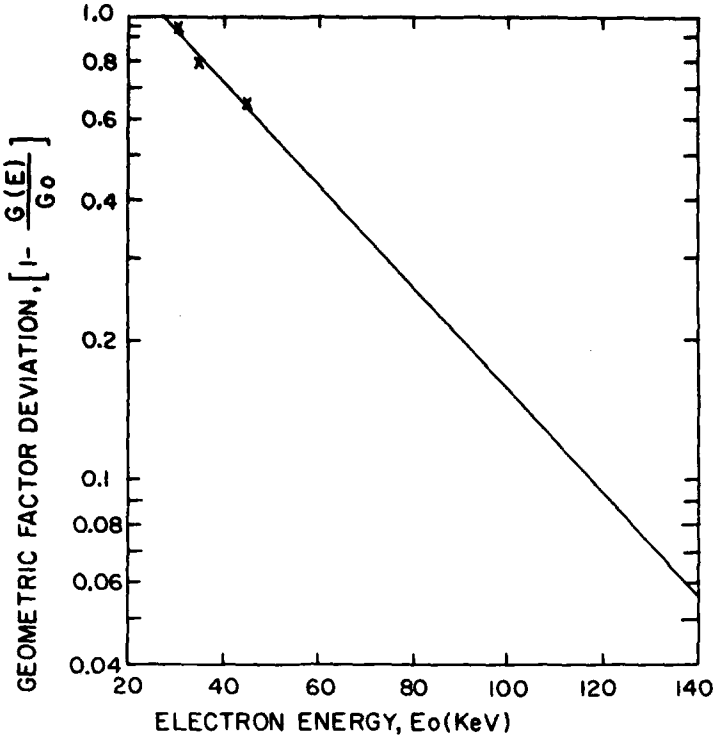

Figure 15. Effective Electron SSS G Factor as a Function of Incident Electron Energy

The $G_{eff}(E)$ in Table 7 was used with the energy ranges of Table 6 to calculate the effective $\overline{G\Delta E}$ for each channel, assuming a flat electron spectrum. These are listed in Table 8, along with other properties of the electron SSS channels. It should be noted that because of energy-loss straggling, the edges of the various electron channels are not perfectly sharp. This effect has been neglected in the calculations for Table 8, and is not expected to have a significant effect when calculating electron spectra.

Backscattering may also have some effect on the coincidence channels, but this has not yet been measured. Future tests are planned on the backup SCATHA RSPD, using high energy beta sources to measure the effective G factors for the 1 MeV differential channel.

Table 8. Summary of Electron SSS Properties

Channel No.	Average Energy (keV)	Channel Width (keV)	Effective $\bar{G}\Delta E$* (cm^2-sr-keV)
A0	39	12	1.21×10^{-2}
A1	58	24	5.12×10^{-2}
A2	96	48	0.144
A3	335	430	1.53
A4	218	95	0.337
C0	>950	-	3.55×10^{-3}+
C1	1040	120	4.26×10^{-1}
C2	70-950	-	3.55×10^{-3}+
C3	>950	-	3.55×10^{-3}+
C4	1040	120	4.26×10^{-1}

*Calculated for a flat electron spectrum.
+These values are cm^2-sr for G(>E), or G(E_1 to E_2).

5.2 Proton SSS G Factors

The proton SSS's, illustrated in Figure 3, are solid state detector telescopes with the G factor determined by an inner collimator of 0.249-cm diam and an outer collimator of 1.300-cm diam, separated by 3.11 cm. This gives $G = 6.69 \times 10^{-3} cm^2$-sr for protons, and since protons scatter far less than electrons, it should be a valid G for the entire energy range of interest.

The most important requirement in calculating the energy response of the proton SSS's is knowledge of the precise front-detector thicknesses. For the flight unit RSPD the $\parallel$ proton SSS has a 6.3-μ-thick front detector, and the $\perp$ proton SSS has a 5.3-μ-thick front detector. These were directly measured by x-ray transmission as described in Ref. 14. Both detectors have a light shield of 116 $\mu g/cm^2$ of Al over the Si surface facing out. The proton responses were calculated using these thicknesses and the energy loss calculations of Ref. 15. The results are presented in Table 9. Because of the thinness of the $\perp$ front detector, the C4 channel does not detect protons, except for a small number, because of

14. Hanser, F.A., and Sellers, B. (1974) Measurement of totally depleted silicon solid state detector thickness by x-ray attenuation, Rev. Sci. Instrum. 45:226.

15. Janni, J.F. (1966) Calculations of Energy Loss, Range, Pathlength, Straggling, Multiple Scattering, and the Probability of Inelastic Nuclear Collisions for 0.1- to 1000-MeV Protons, Rep. AFWL-TR-65-150, AFWL, Kirtland AFB, New Mexico.

straggling in the energy-loss distributions. A summary of the proton SSS properties and the approximate response for the ⊥ C4 channel are shown in Table 10.

Table 9. Detection Energy Ranges for Proton SSS's

Channel No.	Logic Configuration*	Proton Energy Range (keV)+	
		∥ SSS	⊥ SSS
Anticoincidence			
A0	$F_1 \cdot \bar{F}_2 \cdot \bar{R}_1$	101-150	
A1	$F_2 \cdot \bar{F}_3 \cdot \bar{R}_1$	150-225	
A2	$F_3 \cdot \bar{F}_4 \cdot \bar{R}_1$	225-325	
A3	$F_4 \cdot \bar{F}_5 \cdot \bar{R}_1$	325-450	
A4	$F_5 \cdot \bar{F}_6 \cdot \bar{R}_1$	450-547	450-479
Coincidence			
C0	$F_1 \cdot \bar{F}_2 \cdot R_1$	4250-8610	3290-6750
C1	$F_2 \cdot \bar{F}_3 \cdot R_1$	1870-4250	1460-3290
C2	$F_3 \cdot \bar{F}_4 \cdot R_1$	959-1870	733-1460
C3	$F_4 \cdot \bar{F}_5 \cdot R_1$	598-959	491-733
C4	$F_5 \cdot \bar{F}_6 \cdot R_1$	547-598	(-)

*The front (F) and rear (R) detector thresholds are, in kev: F_1=60, F_2=103, F_3=183, F_4=228, F_5=419, F_6=750, R_1=50.

+$G(E)=6.69 \times 10^{-3} cm^2$-sr within the listed energy ranges.

Table 10. Summary of Proton SSS Properties

Channel No.	∥ Proton SSS			⊥ Proton SSS		
	Av. E(keV)	Width(keV)	$\bar{G}\Delta E(cm^2\text{-}sr)$*	Av. E(keV)	Width(keV)	$\bar{G}\Delta E(cm^2\text{-}sr)$*
A0	126	49	0.328	126	49	0.328
A1	188	75	0.502	188	75	0.502
A2	275	100	0.669	275	100	0.669
A3	388	125	0.836	388	125	0.836
A4	499	97	0.644	465	29	0.194
C0	6430	4360	29.1	5020	3460	23.1
C1	3060	2380	15.9	2380	1830	12.2
C2	1410	910	6.07	1100	731	4.89
C3	779	361	2.42	612	242	1.62
C4	573	51	0.341	485	≃10	≃0.01

*Calculated for a flat proton spectrum.

6. ADDITIONAL EFFORT

Three additional required tasks have also been completed. The investigation of the effectiveness of radiation-hardened CMOS in improving RSPD reliability has been completed; the RSPD has been integrated into the SCATHA satellite; and on-site assistance was provided at the Air Force Satellite Control Facility (SCF) for turn-on and initial in-orbit operations of the RSPD in the SCATHA satellite.

The radiation susceptibility of the RSPD was investigated in detail. It was initially concluded that an additional 220 grams of shielding material was desirable, but the spacecraft integrator did not allow this additional weight. The most susceptible direction is, however, shielded by other satellite instruments that were neglected in the first analysis, so the lack of this additional shielding is not critical. The most radiation-sensitive components (two LM 139s) were provided with additional radiation shielding, as were two of the ESA preamplifiers that were the least shielded. The radiation-hardened CMOS are not expected to be a problem. The RSPD should operate reliably in orbit for in excess of 1 year, based on the presently expected radiation environment.

The flight unit RSPD was integrated into the SCATHA satellite, and all necessary testing supported by the appropriate personnel. The satellite was successfully launched on 30 January 1979, and is presently in final orbit.

The RSPD, known as SC5 on the SCATHA satellite, was first turned on on 9 February 1979. The RSPD has operated reliably since then, although some degradation has been observed in some of the SEM's. The SSS's are operating

properly and are on continuously. The ESA's are presently operating at a higher bias level to increase the gain, and are being turned on only about 50 percent of the time. This latter mode of operation is being used since it has been found that the SEM gain recovers when the ESA's are off, and their lifetime can thus be extended by this operation mode. Extensive on-site support at the Air Force Satellite Control Facility in Sunnyvale, CA, was given during the initial turn-on and subsequent real-time operations of the RSPD (SC5).

7. CONCLUSIONS

The Rapid Scan Particle Detector (RSPD) responses have been calculated and, for most of the lower energy channels, calibrated at the Rice University Facility. Detailed response curves have been obtained for all the ESA channels, with only the highest and some of the lowest energy channels having response curves based on extrapolation from the other channels. The electron solid state spectrometers (SSS's) have had their detailed responses calculated and corrected for electron scattering in the lowest energy channels by calibration. The proton SSS's have had their detailed responses calculated based on the detector thicknesses measured by x-ray attenuation.

The RSPD has been integrated into the SCATHA satellite, and is operating properly after turn-on in the satellite's final orbit. The RSPD is presently operating with the SSS's on full-time and the ESA's on about 50 percent of the time to conserve SEM lifetime. Extensive on-site support of RSPD real-time operations at the Air Force Satellite Control Facility in Sunnyvale, CA, has been provided.

References

1. Hunerwadel, J.L., Morel, P.R., Hanser, F.A., and Sellers, B. (1975) Design of Instrumentation Suitable for the Investigation of Charge Buildup Phenomena at Synchronous Orbit, AFCRL-TR-75-0365, Scientific Report No. 1 for Contract No. F19628-74-C-0217, AD A015063.

2. Hunerwadel, J.L., Morel, P.R., Hanser, F.A., and Sellers, B. (1976) Design of Instrumentation Suitable for the Investigation of Charge Buildup Phenomena at Synchronous Orbit, AFGL-TR-76-0263, Scientific Report No. 2 for Contract No. F19628-74-C-0217, AD A034382.

3. Sellers, B., Hanser, F.A., Morel, P.R., Hunerwadel, J.L., Pavel, A.L., Katz, L., and Rothwell, P.L. (1976) A high-time resolution spectrometer for 0.05 to 500 keV electrons and protons, in Spacecraft Charging by Magnetospheric Plasmas, A. Rosen, Editor; AIAA, NY.

4. Archuleta, R.J., and DeForest, S.E. (1971) Efficiency of channel electron multipliers for electrons of 1-50 keV, Rev. Sci. Inst. 42:89.

5. Bordoni, F. (1971) Channel electron multiplier efficiency for 10-1000 eV electrons, Nucl. Inst. Meth. 97:405.

6. Arnoldy, R.L., Isaacson, P.O., Gats, D.F., and Choy, L.W. (1973) The calibration of electrostatic analyzers and channel electron multipliers using laboratory simulated omnidirectional electron beams, Rev. Sci. Inst. 44:172.

7. Iglesias, G.E., and McGarity, J.O. (1971) Channel electron multiplier efficiency for protons of 0.2-10 keV, Rev. Sci. Inst. 42:1728.

8. Egidi, A., Marconero, R., Pizzella, G., and Sperli, F. (1969) Channeltron fatigue and efficiency for protons and electrons, Rev. Sci. Inst. 40:88.

9. Berger, M.J., and Seltzer, S.M. (1966) Additional Stopping Power and Range Tables for Protons, Mesons, and Electrons, Rep. NASA SP-3036, NASA, Washington, DC.

10. Berger, M.J., and Seltzer, S.M. (1964) Tables of Energy Losses and Ranges of Electrons and Positrons, Rep. NASA SP-3012, NASA, Washington, DC.

11. Berger, M.J., Seltzer, S.M., Chappell, S.E., Humphreys, J.C., and Motz, J.W. (1969) Response of silicon detectors to monoenergetic electrons with energies between 0.15 and 5.0 MeV, Nucl. Inst. and Meth. 69:181.

12. Seltzer, S.M., and Berger, M.J. (1974) Transmission and reflection of electrons by foils, Nucl. Instr. and Meth. 119:157.

13. Chappell, S.E., Humphreys, J.C., Motz, J.W., Berger, M.J., and Seltzer, S.M. (1968) Response of silicon transmission detectors to monoenergetic electrons, IEEE Trans. Nucl. Sci. NS-15:359.

14. Hanser, F.A., and Sellers, B. (1974) Measurement of totally depleted silicon solid state detector thickness by x-ray attenuation, Rev. Sci. Instrum. 45:226.

15. Janni, J.F. (1966) Calculations of Energy Loss, Range, Pathlength, Straggling, Multiple Scattering, and the Probability of Inelastic Nuclear Collisions for 0.1- to 1000-MeV Protons, Rep. AFWL-TR-65-150, AFWL, Kirtland AFB, New Mexico.

Appendix A

The Geometric Factors as a Function of Energy

Table A1. Low Energy ESA Geometric Factors – Energy Channel No. 1

Particle Energy E(keV)	∥ LE ESA G(E)*		⊥ LE ESA G(E)*	
	Electron	Proton	Electron	Proton
0.03	3.-8	5.-8	3.-8	3.-8
0.04	1.48-7	1.2-7	6.0-7	7.-8
0.05	4.2-5	3.5-7	4.7-5	2.2-7
0.06	8.7-5	5.-6	1.11-4	3.0-6
0.07	9.5-5	7.-5	9.2-5	5.2-5
0.08	1.00-4	1.8-4	7.3-5	1.03-4
0.09	8.7-5	2.0-4	7.-5	1.18-4
0.10	8.1-5	2.0-4	6.-5	1.2-4
0.12	5.5-5	2.0-4	3.-5	1.15-4
0.15	2.5-5	1.75-4	1.56-5	8.7-5
0.2	8.0-6	5.3-5	6.8-6	3.5-5
0.3	1.0-6	3.9-6	1.2-6	2.7-6
0.4	4.7-7	5.3-7	8.-7	8.8-7
0.5	3.7-7	5.8-7	7.-7	8.5-7
0.7	3.4-7	6.5-7	7.-7	8.5-7
1.	7.9-7	7.5-7	8.-7	9.-7
3.	1.3-6	1.6-6	1.2-6	1.1-6
10.	1.3-6	1.7-6	1.4-6	1.2-6
30.	1.3-6	2.1-6	1.5-6	1.1-6
100.	1.3-6	2.5-6	1.4-6	1.1-6

*G(E) in cm^2-sr; 3.-8≡3×10^{-8}, etc.

Table A2. Low Energy ESA Geometric Factors – Energy Channel No. 2

Particle Energy E(keV)	↑ LE ESA G(E)*		↓ LE ESA G(E)*	
	Electron	Proton	Electron	Proton
0.09	3.-8	9.-8	3.-8	4.5-8
0.10	2.5-7	1.3-7	1.5-7	7.0-8
0.13	7.5-5	1.0-6	9.0-5	5.0-7
0.15	1.09-4	1.36-5	1.46-4	8.0-6
0.17	1.2-4	8.8-5	1.43-4	5.5-5
0.20	1.30-4	1.16-4	1.23-4	8.5-5
0.25	1.05-4	1.5-4	8.7-5	9.5-5
0.30	7.7-5	1.5-4	5.7-5	8.7-5
0.35	4.5-5	1.2-4	4.0-5	7.2-5
0.40	3.0-5	8.8-5	2.2-5	5.5-5
0.5	9.0-6	4.4-5	8.5-6	2.2-5
0.7	1.4-6	4.7-6	2.2-6	2.4-6
1.	7.5-7	1.0-6	1.2-6	6.7-7
2.	1.2-6	1.2-6	1.1-6	6.7-7
5.	1.7-6	1.5-6	1.6-6	7.7-7
10.	1.8-6	1.5-6	1.9-6	8.0-7
30.	1.3-6	2.1-6	1.4-6	8.5-7
100.	1.3-6	2.5-6	2.2-6	8.5-7

*G(E) in cm^2-sr; 3.-8≡3.x10^{-8}, etc.

Table A3. Low Energy ESA Geometric Factors – Energy Channel No. 3

Particle Energy E(keV)	∥ LE ESA G(E)*		⊥ LE ESA G(E)*	
	Electron	Proton	Electron	Proton
0.1	3.-8	3.-8	3.-8	3.-8
0.2	3.-8	1.-7	3.-8	5.-8
0.25	6.2-7	2.2-7	1.2-8	1.2-7
0.3	5.8-5	6.2-7	4.1-5	4.0-7
0.35	1.26-4	1.6-5	1.14-4	6.5-6
0.4	1.45-4	1.54-4	1.06-4	8.0-5
0.5	1.49-4	2.3-4	9.4-5	1.3-4
0.6	1.2-4	2.3-4	7.4-5	1.35-4
0.7	9.1-5	1.99-4	4.9-5	1.25-4
0.8	6.0-5	1.7-4	3.1-5	1.1-4
1.0	2.5-5	8.6-5	9.5-6	6.3-5
1.5	3.1-6	3.5-6	1.5-6	8.0-6
2.	1.1-6	1.5-6	4.4-7	1.2-6
3.	1.3-6	1.4-6	6.0-7	9.8-7
5.	1.2-6	1.6-6	7.5-7	1.0-6
10.	1.6-6	1.7-6	1.1-6	1.2-6
30.	1.7-6	2.1-6	2.1-6	1.3-6
100.	1.3-6	2.5-6	1.4-6	1.3-6

*G(E) in cm^2-sr; 3.-8≡3. x'0^{-8}, etc.

Table A4. Low Energy ESA Geometric Factors – Energy Channel No. 4

Particle Energy E(keV)	↑ LE ESA G(E)*		↓ LE ESA G(E)*	
	Electron	Proton	Electron	Proton
0.1	3.-8	3.-8	3.-8	3.-8
0.4	1.1-7	8.-8	3.-8	4.5-8
0.5	1.8-6	1.8-7	5.6-7	9.0-8
0.6	1.3-5	3.7-7	1.-6	2.3-7
0.7	5.5-5	2.5-6	9.4-6	8.0-7
0.8	1.09-4	3.0-5	7.6-5	1.0-5
0.9	1.3-4	2.1-4	1.17-4	9.0-5
1.0	1.39-4	3.1-4	1.39-4	1.5-4
1.2	1.3-4	2.9-4	1.32-4	1.8-4
1.5	1.03-4	2.5-4	9.8-5	1.8-4
2.0	4.9-5	1.4-4	4.3-5	1.2-4
2.5	1.6-5	7.-5	1.8-5	5.8-5
3.	5.8-6	2.8-5	6.0-6	2.3-5
4.	1.5-6	2.5-6	2.3-6	2.9-6
5.	1.7-6	1.9-6	2.4-6	1.4-6
7.	1.3-6	1.6-6	1.0-6	1.3-6
10.	1.6-6	1.8-6	1.0-6	1.3-6
30.	1.6-6	2.1-6	1.4-6	1.5-6
100.	1.3-6	2.5-6	1.7-6	1.6-6

*G(E) in cm^2-sr; 3.-8≡3.x10^{-8}, etc.

Table A5. High Energy ESA Geometric Factors – Energy Channel No. 1

Particle Energy E(keV)	∥ HE ESA G(E)*		⊥ HE ESA G(E)*	
	Electron	Proton	Electron	Proton
0.1	1.-8	3.-8	3.-8	3.-8
0.5	3.-8	3.-8	3.-8	3.-8
0.7	7.1-8	4.4-8	9.9-8	3.7-8
1.0	1.1-6	1.2-7	7.1-7	1.1-7
1.5	4.8-6	1.5-6	2.7-6	2.3-6
2.0	3.2-5	2.0-5	2.4-5	9.5-6
2.5	3.8-5	2.3-4	2.9-5	2.7-4
3.	3.8-5	2.7-4	2.9-5	3.0-4
4.	2.7-5	2.3-4	2.1-5	2.2-4
5.	1.8-5	1.5-4	1.3-5	1.1-4
7.	6.3-6	3.5-5	4.7-6	2.0-5
10.	1.8-6	2.2-6	1.1-6	1.3-6
15.	1.3-6	1.6-6	4.4-7	1.1-6
20.	1.3-6	1.5-6	8.-7	9.2-7
30.	1.1-6	1.4-6	9.5-7	8.-7
100.	1.3-6	1.3-6	8.-7	6.-7

*G(E) in cm^2-sr; 1.-8≡1.x10^{-8}, etc.

Table A6. High Energy ESA Geometric Factors – Energy Channel No. 2

Particle Energy E(keV)	∥ HE ESA G(E)*		⊥ HE ESA G(E)*	
	Electron	Proton	Electron	Proton
0.1	1.-8	1.-8	1.-8	1.-8
1.	1.2-8	1.8-8	3.-8	3.-8
1.5	2.0-7	4.5-8	1.-7	3.-8
2.	8.3-7	3.6-8	4.3-7	1.7-7
3.	5.1-6	4.0-7	3.1-6	7.1-7
4.	1.2-5	4.5-6	7.8-6	5.9-6
5.	2.9-5	4.7-5	2.6-5	1.2-4
6.	3.0-5	2.4-4	2.5-5	2.9-4
7.	2.8-5	3.1-4	2.5-5	3.0-4
8.	2.6-5	3.2-4	2.2-5	3.1-4
10.	1.9-5	2.6-4	1.6-5	2.3-4
15.	5.8-6	9.8-5	4.9-6	5.6-5
20.	1.3-6	5.8-6	2.4-6	2.5-6
25.	1.9-6	2.5-6	1.6-6	1.4-6
30.	1.3-6	2.3-6	1.1-6	1.3-6
40.	1.4-6	1.9-6	9.4-7	1.1-6
50.	1.3-6	1.8-6	7.-7	1.0-6
100.	1.3-6	1.6-6	7.-7	8.-7

*G(E) in cm^2-sr; 1.-8≡1.x10^{-8}, etc.

Table A7. High Energy ESA Geometric Factors – Energy Channel No. 3

Particle Energy E(keV)	∥ HE ESA G(E)*		⊥ HE ESA G(E)*	
	Electron	Proton	Electron	Proton
0.1	1.-8	1.-8	1.-8	1.-8
1.	2.7-8	1.-8	1.-8	1.-8
2.	3.-8	2.-8	2.-8	1.-8
3.	1.7-7	3.-8	3.-8	1.9-8
4.	5.7-7	5.-8	4.-7	3.5-8
5.	1.4-6	9.-8	1.-6	7.2-8
6.	3.2-6	2.1-7	2.3-6	1.9-7
7.	4.3-6	3.3-7	3.5-6	3.6-7
8.	5.9-6	8.9-7	5.7-6	1.3-6
10.	1.2-5	5.5-6	7.4-6	7.1-6
12.	2.0-5	4.5-5	1.5-5	8.5-5
15.	2.6-5	2.5-4	1.8-5	3.1-4
20.	2.2-5	3.2-4	1.8-5	2.8-4
25.	1.8-5	2.5-4	1.4-5	2.0-4
30.	1.2-5	1.6-4	9.0-6	1.0-4
40.	3.3-6	5.5-5	3.2-6	3.3-5
50	1.8-6	3.5-6	1.7-6	2.0-6
60.	1.4-6	2.5-6	1.2-6	1.3-6
70.	1.3-6	2.2-6	9.-7	1.2-6
100.	1.3-6	1.8-6	6.-7	1.-6

*G(E) in cm^2-sr; 1.-8≡1.x10^{-8}, etc.

Table A8. High Energy ESA Geometric Factors – Energy Channel No. 4

Particle Energy E(keV)	∥ HE ESA G(E)*		⊥ HE ESA G(E)*	
	Electron	Proton	Electron	Proton
0.1	1.-8	1.-8	1.-8	1.-8
5.	2.-8	1.-8	3.-8	1.-8
7.	9.5-8	3.-8	9.-8	3.-8
10.	4.9-7	6.8-8	2.6-7	1.4-7
15.	2.0-6	2.1-7	1.5-6	2.-7
20.	4.9-6	6.8-7	4.7-6	1.3-6
25.	9.5-6	9.5-6	7.3-6	1.5-5
30.	1.51-5	7.2-5	1.22-5	1.48-4
40	1.67-5	3.0-4	1.4-5	2.9-4
50.	1.4-5	3.0-4	1.25-5	2.6-4
60.	1.1-5	2.4-4	9.5-6	1.9-4
70.	8.0-6	1.8-4	7.0-6	1.3-4
80.	5.3-6	1.3-4	4.5-6	8.2-5
100.	2.0-6	4.5-5	2.1-6	2.3-5
120.	1.3-6	5.-6	1.4-6	1.8-6
150.	1.3-6	2.5-6	9.-7	1.3-6
200.	1.3-6	2.-6	6.-7	1.1-6

*G(E) in cm^2-sr; 1.-8≡1.x10^{-8}, etc.